

We are IntechOpen, the world's leading publisher of Open Access books Built by scientists, for scientists

6,900

Open access books available

185,000

International authors and editors

200M

Downloads

Our authors are among the

154

Countries delivered to

TOP 1%

most cited scientists

12.2%

Contributors from top 500 universities



WEB OF SCIENCE™

Selection of our books indexed in the Book Citation Index
in Web of Science™ Core Collection (BKCI)

Interested in publishing with us?
Contact book.department@intechopen.com

Numbers displayed above are based on latest data collected.
For more information visit www.intechopen.com



Getting Charged for the Mitochondrial Uptake

Ivo Crnolatac

Abstract

Mitochondria are hot! First of all, literally. Recent results showed that locally in the functional human mitochondria, the temperature rises close to 50°C. The research was based on the thermosensitive fluorescent dye that targets mitochondria. Figuratively, mitochondria are even hotter, in terms of undergoing research exploring their role in energy production, cell signalling, programmed cell death and biosynthesis. Fluorescent probes and dyes are not restricted only to imaging of these fascinating organelles; they are used to monitor the mitochondrial membrane potential, pH and the redox status. The membrane potential is essential in the process of ATP production as it constitutes more than 80% of electrochemical proton motive force used in this process. Thus, observing mitochondrial membrane potential is crucial in most of the mitochondrial research. This imaging should usually be performed with minimal invasiveness and damage to the mitochondria and mitochondrial function. There are only a few fluorescent probes for mitochondrial membrane potential monitoring currently in use as valuable indicators of cells' functional status. Those probes show varying degrees of interference with cell or mitochondrial metabolism and photo-induced damage. In this chapter, the characteristics, advantages and disadvantages of such probes will be discussed. The mechanisms of uptake of these fluorescent probes will be explained.

Keywords: mitochondria, fluorescent probes, morphology, membrane potential, fluorescent sensor, superoxide anion, hydrogen peroxide

1. Introduction

Previously, mitochondria were studied exclusively in terms of bioenergetics. However, the so-called powerhouse of the cell, apart from producing adenosine triphosphate (ATP) by oxidative phosphorylation, takes part in numerous metabolic pathways. Apoptosis signalling [1, 2], ageing [3, 4], calcium homeostasis [5, 6] and cell development [7, 8] are also responsibilities of this remarkable cell organelle. Thus, to no surprise, the pathogenesis of many diseases stems from mitochondrial dysfunction, for instance, Alzheimer type dementia [9] and other neurodegenerative diseases [10] as well as cancer [11]. The relation between mitochondria and cancer goes well beyond excessive reactive oxygen species (ROS) production by Complex I and Complex III of the electron transfer chain (ETC). The differences in mitochondrial activity between healthy and cancer cells include metabolic variances [12], mostly due to the shift to glycolytic metabolism. Various cancers reportedly have mutations and alternations in the mtDNA, with the D-loop region of mtDNA bearing most of these mutations [12]. The mutations in nuclear DNA that encodes

for mitochondrial proteins are also observed in cancer cells. However, there is strong indication that those mutations are the result of intergenomic cross-talk between mitochondria and nucleus and also originate from mutations in mtDNA [13]. Another fascinating feature of mitochondria is the interchanging processes of fusion and fission. This mitochondrial dynamics enables the control of the metabolic pathways mentioned at the beginning of this paragraph [14]. Shifting of the fission-fusion equilibrium is also the way of adaptation to physiological changes and environmental stress [14].

Although studying the biology and biochemistry of mitochondria is captivating and rewarding, the main topic in this chapter will be the fluorescent probes and dyes targeting mitochondria, the comprehensive overview of available fluorescent compounds that allow characterisation of mitochondria, and study of its functionality. Sections will cover main groups of compounds according to their applications in mitochondrial cell biology and biochemistry. Mitochondrial markers are used to fluorescently label the mitochondria and enable visualisation by different fluorescence-based imaging techniques. Monitoring and measuring mitochondrial membrane potential is likewise enabled by specific fluorescent probes. Superoxide indicators will also be covered in a separate section, as will the calcium flux and autophagy probes. Some aspects of mitochondrial uptake will be explained, as that bears an exceptional value in the design of the new potential probes. In the final section, some new perspective probes will be presented, showing exciting features and the possibility of simultaneous dual applicability.

2. Mitochondrial morphology probes

As mentioned in the introductory part, mitochondria are obviously very dynamic organelles. They are undergoing cycles of fusion and fission, transport, processes of biogenesis and mitophagy. These processes are crucial for regulating signalling pathways, regulating mitochondrial turnover, maintaining ETC and mitochondrial homeostasis. Fusion-fission and biogenesis-mitophagy dynamics regulate the morphology, number and transient subcellular localisation of mitochondria. Fluorescent mitochondrial trackers and sensors, enabling real-time monitoring and imaging, were always in demand. Improvements in microscopy have not only instigated more detailed observation and in-depth exploration of mitochondrial dynamics, but also sparked the interest in new sensors.

2.1 Mitochondria-specific fluorescence proteins

The scientists studying mitochondrial dynamics, abundance and morphology in live cells often use specifically targeted fluorescent proteins (FPs). Although the mitochondria evolved from *Alphaproteobacteria* in an endosymbiotic manner within a primordial eukaryotic cell [15], and they possess the whole mechanism for transcription and translation [16], only 13 mitochondrial proteins are produced in the mitochondria [17]. Most of the mitochondrial proteins (>2000) are imported from the cytosol, and the genes encoding them are in the nucleus [18]. So are the mitochondrial targeting signals (MTSs), short (<70) amino acid sequences that direct the synthesised proteins to the specific mitochondrial part. The FP gene is fused with a gene encoding MTS. There are few MTSs that are used frequently. For instance, E1 alpha pyruvate dehydrogenase [19] and cytochrome C oxidase VIII [20] are used by companies for ready-made fluorescent mitochondria targeting reagents [21, 22] and fused plasmids [23]. Beside fluorescent protein and MTS encoding genes, the commercially available constructs contain promoters (usually

Cytomegalovirus, CMV), driving the expression of FP, and antibiotic resistance genes, enabling selective pressure and thus allowing the creation of stable cell lines. Transfection or transduction of these vectors into the targeted cells is achieved using the usual methodology, depending on the cells. The FP methodology is safe as these constructs do not replicate in mammalian cells. It can be used for live cell imaging; however fluorescent signal can also be observed after cell fixation procedure, thus rendering the FPs approach applicable for fixed cells, if the FP expression is achieved before fixation. Flow cytometry using mitochondria targeted GFP has also been reported [24]. The advantages of this technique are: the possibility of targeting specific compartment within mitochondria by choice of targeting signals [25], fewer adverse effects on the observed cells and mitochondria, compared to synthetic fluorescent probes, and relatively stable fluorescence. Disadvantages are related to transfection/transduction efficacy, low levels of FP expression and possible mistargeting, caused probably by the sheer size of the FP. The example of photomicrography depicting HeLa cells stably expressing FP in the mitochondria is presented in **Figure 1**.

2.2 Fluorescent probes targeting mitochondria

As mentioned, fused FPs exploit the fact that their fusion partners, MTSs, are actively transported to mitochondria. Small synthetic fluorescent dyes cannot use that trick. As the mechanism of mitochondrial uptake relates to all small molecules targeting mitochondria, it will be deliberated in more detail in a separate section. **Figure 2** shows commonly used, commercially available compounds [27, 28] and some of the mitochondrial probes designed, synthesised and investigated in collaboration with partners in our laboratory [29–31].

The advantages of this methodology are the ease of use and versatile applicability. Small molecule probes can be used for live cell imaging, fixed cells imaging as well as for flow cytometry. The procedure is as easy as adding the probe in desired concentration to the medium, incubating the cells for designated time and imaging (**Figures 3 and 4**), cell fixation followed by imaging (**Figure 5**) or performing flow cytometry experiment. **Figure 4** portrays cells that are treated with multiple fluorescent probes before

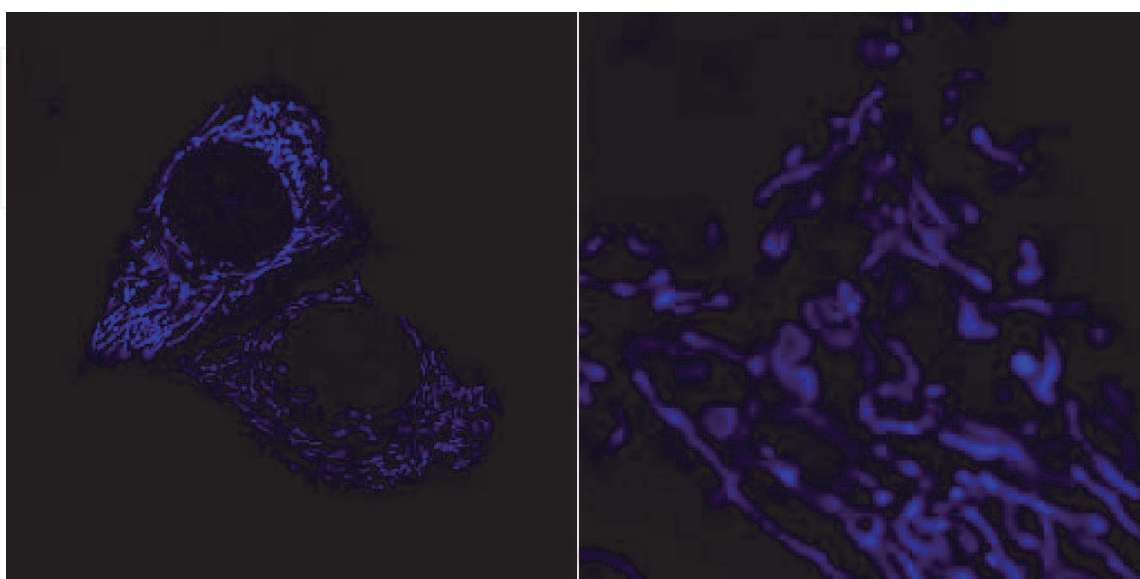


Figure 1. *mitoCFP transfected HeLa cells, expressing mitochondria targeted cyan fluorescence protein (CFP) were seeded on glass-bottom petri dishes (MatTek, USA). After 24 h of cultivation at 37°C in a humidified atmosphere with 5% CO₂, cells were analysed using a confocal microscope (Leica TCS SP2 AOBS), with $\lambda_{EX} = 458\text{ nm}$, emission was detected with a bandpass filter at 470–510 nm [26].*

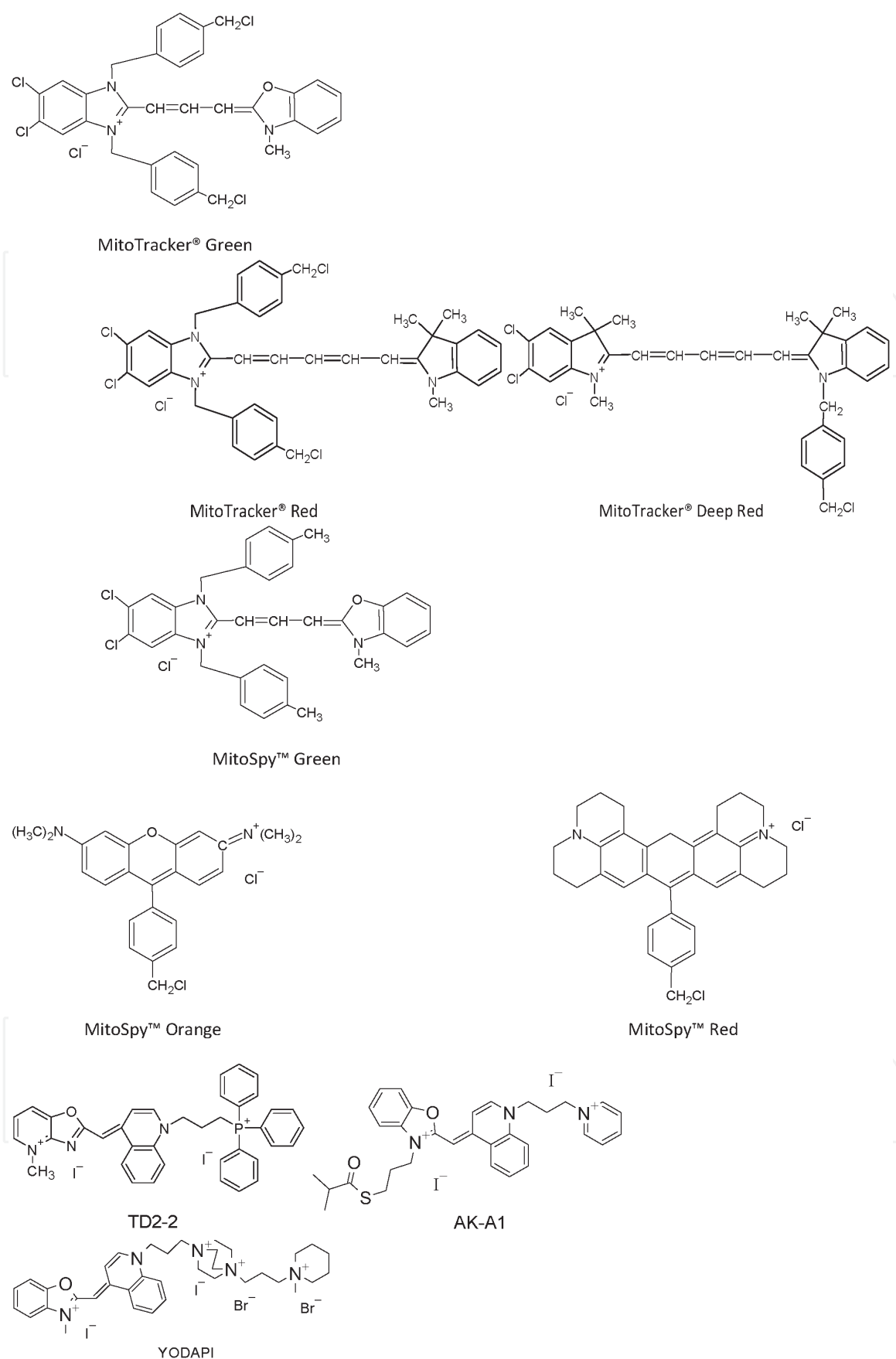


Figure 2. Structures of the commonly used, commercially available mitochondrial fluorescent probes and some of our cyanine probes that successfully target mitochondria.

imaging. Such methodology is used for colocalisation purposes, to verify the localisation of one of the colocalising partners (**Figures 4(A)** and **6**), or to visualise mitochondria in relation to other cellular organelles and cellular processes (other

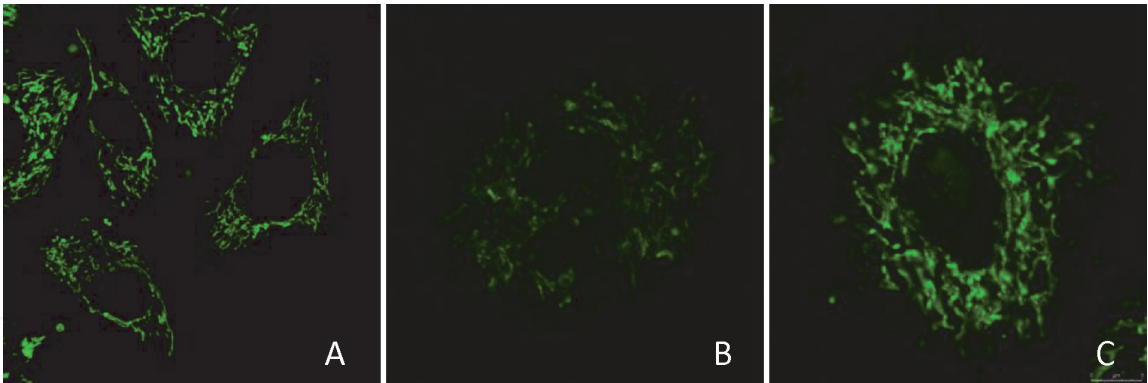


Figure 3. Live cell images of the cells after exposure to the mitochondria targeting fluorescent probes. (A) HeLa cells incubated for 120 min with 1×10^{-6} Mol/dm³ TD2-2. $\lambda_{EX} = 514$ nm and $\lambda_{EM} = 540\text{--}620$ nm. (B) H460 cells incubated for 120 min with 1×10^{-6} Mol/dm³ AK-A1, $\lambda_{EX} = 483$ nm and $\lambda_{EM} = 499\text{--}522$ nm. (C) H460 cells incubated for 120 min with 1×10^{-6} Mol/dm³ of YODAPI, $\lambda_{EX} = 482$ nm and $\lambda_{EM} = 498\text{--}535$ nm.

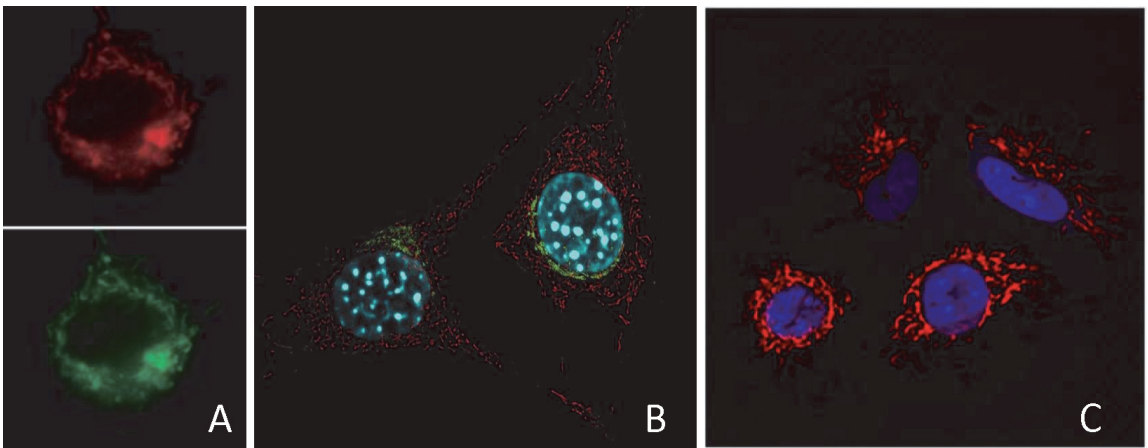


Figure 4. (A) Images of an NIH 3 T3 cell showing colocalisation of the CoroNa™ Red sodium indicator with the MitoTracker® Green FM mitochondrial marker. A cell loaded with both dyes was imaged consecutively using omega optical bandpass filter set XF41 for CoroNa™ Red sodium indicator and set XF23 for MitoTracker® Green FM. (B) Live NIH 3 T3 cells labelled with probes for mitochondria, Golgi and the nucleus. Mitochondria were labelled with MitoTracker® Red FM, Golgi with BODIPY® FL ceramide, and the nucleus with Hoechst 33342. The image was deconvolved using Huygens software (scientific volume imaging). (C) HeLa cells were co-transduced with CellLight® Nucleus-CFP and incubated overnight. Following staining with MitoTracker® deep red, cells were imaged on a Zeiss 710 confocal microscope. Images and captions are displayed with the permission of Thermo Scientific.

images in **Figure 4**). As the visual comparison of the colocalisation images is subjective due to the different intensity of the fluorescence signal emitted by the two dyes, simply overlapping the images is usually not sufficient for evaluation. The colocalisation is often quantified using a pixel-by-pixel summation of the products of the intensities of two fluorophores, the Pearson correlation coefficient (PCC, r) [32]. In the case of green pixels G_i and red pixels R_i :

$$r = \frac{\sum (R_i - Rav) * (G_i - Gav)}{\sqrt{\sum (R_i - Rav)^2 * \sum (G_i - Gav)^2}} \tag{1}$$

The software packages available for processing microscopy images usually have implemented options for PCC calculation, and so does the most frequently used open-source software, ImageJ [33]. However, PCC, due to the photon noise is not flawless. This noise can be diminished by extending the image acquisition time, by binning adjacent pixels or by summing replicate images. Still, the replicate-based

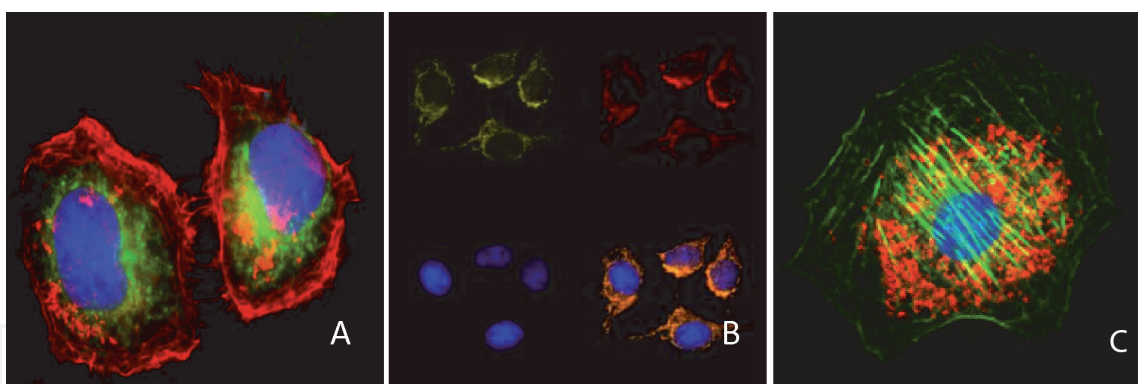


Figure 5.

(A) HeLa cells were stained with 250 nM of **MitoSpy™ Green FM** (green) for 20 min and fixed with 4% paraformaldehyde (PFA) for 10 min. Then the cells were stained with Alexa Fluor® 594 phalloidin for 20 min (red) and counterstained with DAPI (blue). The image was captured with a 60× objective. (B) HeLa cells were stained with 250 nM of **MitoSpy™ Orange CMTMR** (yellow) for 20 min, fixed with 4% paraformaldehyde (PFA) for 10 min, and permeabilised with 0.1% triton X-100 for 10 min. Then the cells were stained with anti-cytochrome C Alexa Fluor® 647 (red) and counterstained with DAPI (blue). All three images were merged in the bottom right panel. The image was captured with a 60× objective. (C) NIH3T3 cells were stained with 100 nM of **MitoSpy™ red** (red) for 20 min at 37°C, fixed with 1% paraformaldehyde (PFA) for 10 min at room temperature, and permeabilised with 1X True Nuclear™ Perm Buffer for 10 min at room temperature. Then the cells were stained with flash Phalloidin™ NIR 647 (green) for 20 min at room temperature and counterstained with DAPI (blue). The image was captured with a 60× objective. Images and captions are displayed with the permission of BioLegend.

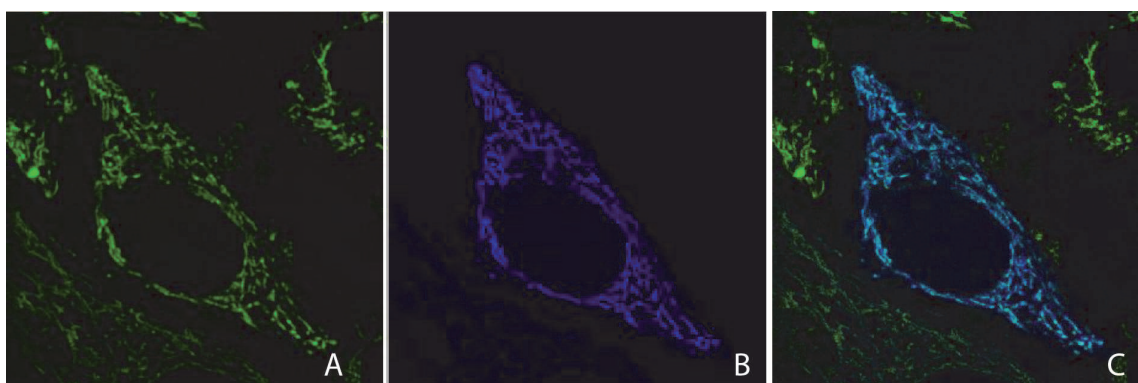


Figure 6.

Confocal photofluoromicrographs of HeLa cells expressing mitochondria targeted CFP and incubated for 120 min with compound TD2-2. (A) Fluorescence emitted by the TD2-2, $\lambda_{EX} = 514$ nm and $\lambda_{EM} = 540-620$ nm. (B) Fluorescence emitted by CFP, $\lambda_{EX} = 458$ nm and $\lambda_{EM} = 470-510$ nm. (C) Represents overlayed images (A) and (B).

noise correction correlation (RBNCC) offers excellent results without implementing complicated or time-consuming actions [34]. Shortly, in the case of green and red channels, two consecutive images are taken, and correction factor (r_{GR}) is calculated from those two consecutive green/red channel images. Noise-corrected PCC (r_{corr}) is the product of the mean of four green/red combinations with the above-explained correction, as described in **Figure 7**.

$$r_{corr} = r_{GR} * \frac{(r_{G1R1} + r_{G1R2} + r_{G2R1} + r_{G2R2})}{4} \quad (2)$$

Multiple staining can also be achieved for live cell imaging (**Figures 4 and 6**). In general, these compounds are all hydrophobic, and therefore usually not soluble in aqueous media, but they are readily soluble in dimethylsulphoxide (DMSO). The concentration of the DMSO stock solutions should be high enough not to exceed the cell culture tolerance on DMSO. The DMSO content in the medium that does not

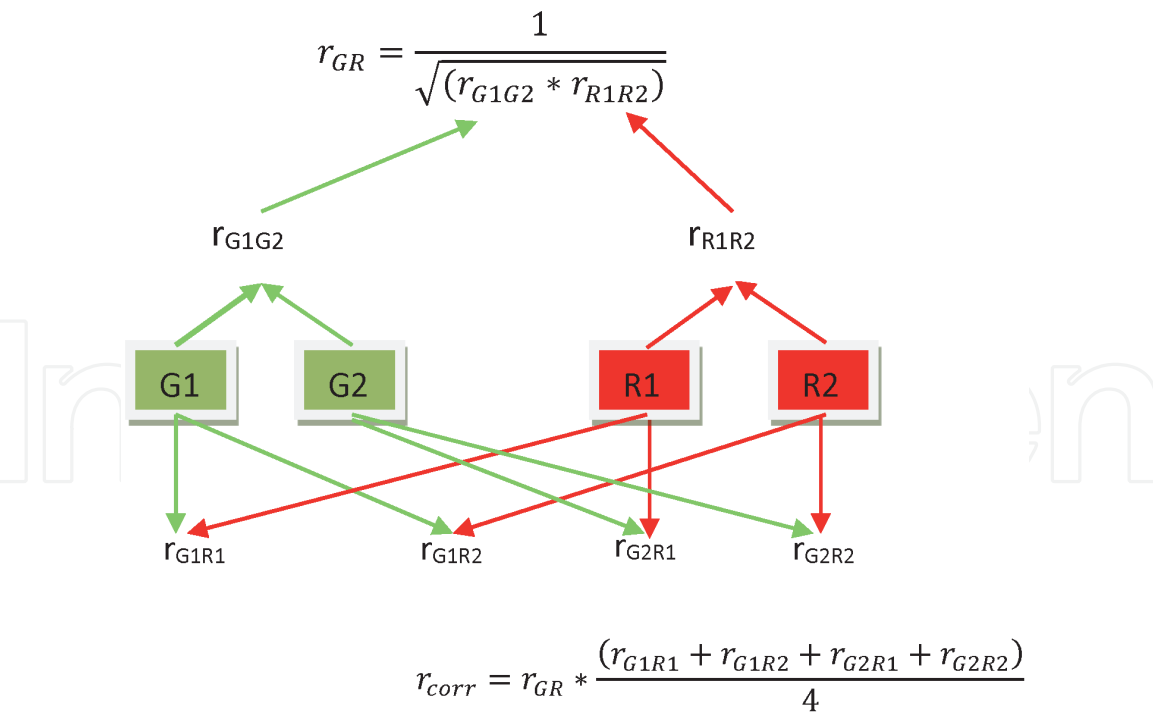


Figure 7.
Schematic description of RBNCC calculation.

affect the cells is cell type dependent, but as a rule of thumb, it should not exceed 0.1–0.5%. Various detrimental effects on the mitochondria and, consequently, on cells are the main disadvantages of these probes, along with non-specific accumulation (**Figure 3(C)**, nucleus) and photobleaching [35].

3. Charge, lipophilicity: keys for the mitochondrial uptake

Synthetic fluorescent probes have to enter the cell and navigate towards mitochondria, pass outer and inner mitochondrial membranes to enter the matrix. So what is the driving force, which attracts and internalises these compounds? The quest for the answer starts with the inspection of the structural similarities. Most of the presented compounds in **Figure 2** are, in fact, cyanine dyes, but that has more to do with their tunable spectroscopic and fluorescence properties [36]. The main features determining them for mitochondrial uptake are lipophilicity and charge. They all are highly lipophilic cations (LC), some of them multiply charged.

Despite the net charge, LCs are lipid-soluble and can move through phospholipid bilayers. As opposed to hydrophilic cations which, unless actively transported by ionophores or carrier proteins, cannot permeate biomembranes. Moving the hydrophilic cation from the aqueous environment into the lipophilic core of the membrane requires too much energy. The activation energy for the movement of LC through the hydrophobic barrier of a biological membrane is lower than for hydrophilic cations. The activation energy for the displacement of a solvated cation from the aqueous milieu to the membrane core consists of electrostatic interactions and hydrophobic forces. The principal electrostatic interaction constituent is Born energy (W_B), the enthalpic penalty of removing the solvating water molecules from the cation upon entering the membrane core [37].

$$W_B = \frac{q^2}{8\pi\epsilon_0 r} \left(\frac{1}{\epsilon_1} - \frac{1}{\epsilon_2} \right) \tag{3}$$

In this equation, ϵ_0 is the vacuum permittivity, ϵ_1 is the dielectric constant of membrane core (~ 2), ϵ_2 is the dielectric constant of water (~ 80), q is the electrical charge per mole of the cation and r is the ionic radius. Thus, the Born energy (W_B) in kJ/mol for a cation with Z charges is given by:

$$W_B = 339 * \frac{Z^2}{r}$$

So the enthalpy needed to transport the cation to the membrane is inversely proportional to the ionic radius. When the charge is distributed on the large surface area, as in all of the structures in **Figure 2**, the cation is less likely to be intensely solvated, as the electric field at the surface is not strong and less water polarisation arises. Apart from Born energy, there are two other electrostatic forces related to the transport of the cations through the biological membranes that are significantly less prominent: dipole energy, caused by the electrical potential within the bilayer, a result of the orientation of the dipoles in phospholipids and image energy, caused by the electrostatic forces at the interface [38]. Those are the forces that work against the transport of the LC to the membrane. The force that lowers the activation energy of the transport and attracts LCs is caused by the increase of entropy due to the loss of the water structure, upon moving a large hydrophobic surface from water to lipid environment. Here, again, the large surface area plays a beneficial role for the transport, contributing with 92 J/mol per \AA^2 of the solvent accessible area [18].

The energy profile for the passage of the LC through the phospholipid bilayer, depicted in **Figure 8**, is assembled, taking into consideration the electrostatic forces and hydrophobic effect. The potential energy wells at both interface surfaces of the membrane are due to the fact that hydrophobic interactions arise with the proximity to the membrane, while the repulsive electrostatic forces increase upon moving through the membrane [40]. Thus, LCs are adsorbed to the membrane surface (usually in monolayers), before fast passage through the core of the membrane to the potential well on the other side followed by slower desorption from the

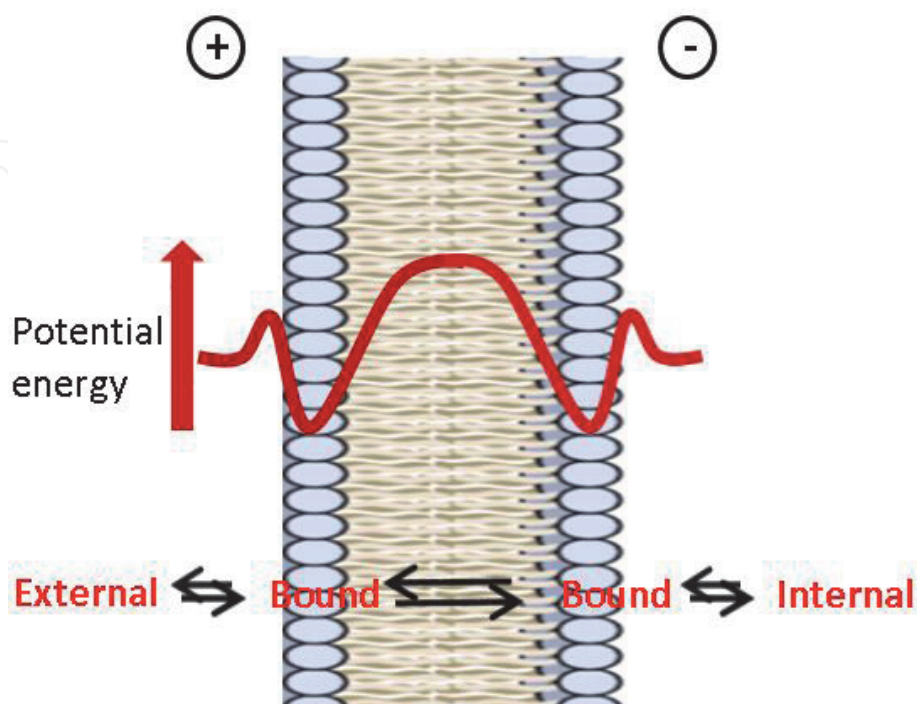


Figure 8.
The energy profile for the passage of the LC through the phospholipid bilayer [39].

membrane. The adsorption can be described by the Langmuir isotherm model assuming the independent binding of the LC to the binding sites on the membrane; in high LC concentrations, repulsive forces between LC molecules have to be considered. The mechanism is spontaneous ($\Delta G_r < 0$), entropy driven ($-T \Delta S_r > \Delta H_r$) and occurs even in the absence of mitochondrial electrochemical proton motive force (Δp) or its major constituent membrane potential ($\Delta \psi_m$, constitutes for >80% of Δp). The $\Delta \psi_m$ is present on the cell membrane (30–60 mV) and inner mitochondrial membrane (150–180 mV) [41], causing several hundredfold accumulation (~10 fold per every 60 mV of $\Delta \psi_m$) of the LC in the mitochondrial matrix following the Nernst equation:

$$\Delta \psi_m = \frac{2.303RT}{F} \log_{10} \left(\frac{[cation_{in}]}{[cation_{out}]} \right)$$

where $\Delta \psi_m$ is the membrane potential, R is the universal gas constant: $R = 8.314 \text{ J/Kmol}$, F is the Faraday constant, the number of coulombs per mole of electrons: $F = 96485.33 \text{ C/mol}$.

4. Membrane potential probes

The flux of protons in the inner membrane of the mitochondria (IMM) is proportional to the mitochondrial respiration rate and can be compared to the simple electrical circuit as depicted in **Figure 9**. Using that analogy, we can describe the Δp as the voltage in the Ohm's law.

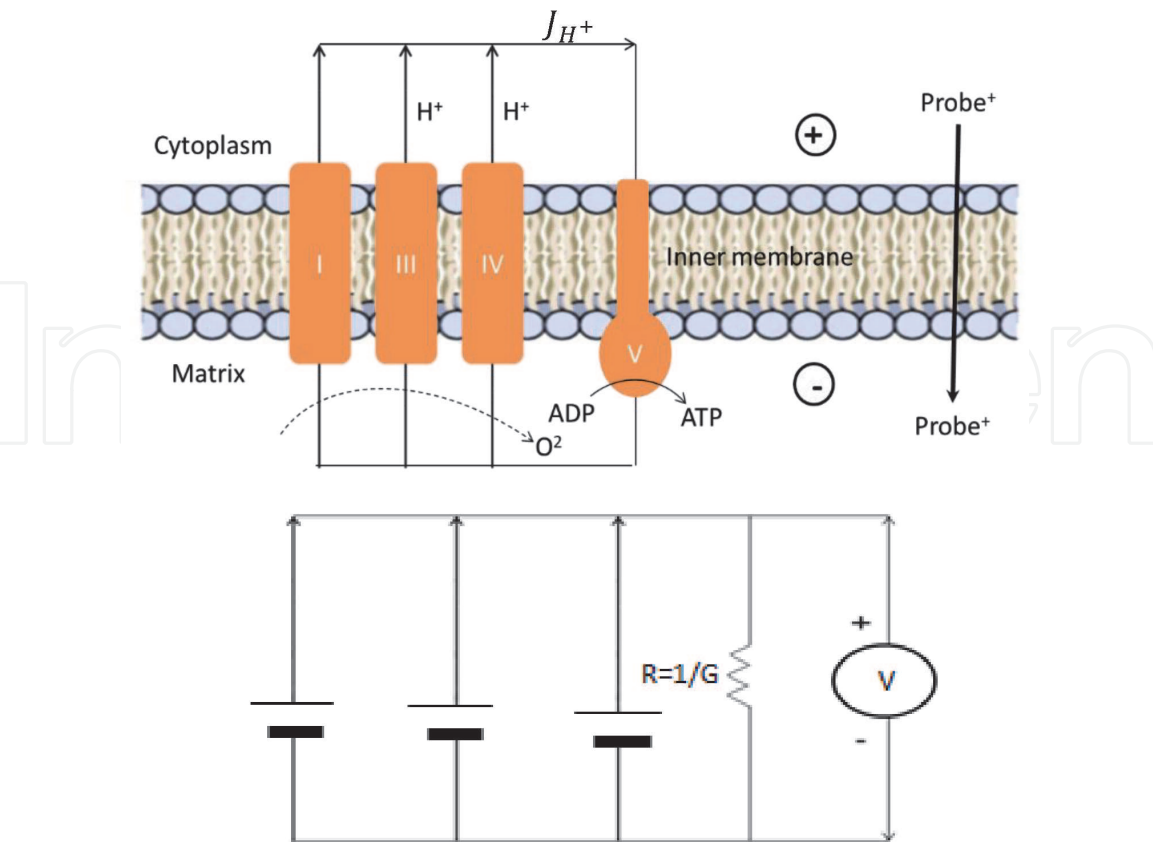


Figure 9. The similarity of the mitochondrial proton flux and the electrical circuit. (UP) Proton flux across the inner mitochondrial membrane, protons are concentrated in the intermembrane space by the protein complexes I, III and IV, to drive the ATP production upon return via complex V. (DOWN) Simple electrical current circuit.

Ohm's law:

$$I = V * G \quad (4)$$

where I is the electrical current, V is the potential difference and G is the conductance, that is reciprocal to resistance.

Proton flux equation:

$$J_{H^+} = \Delta p * C_m H^+ \quad (5)$$

where J_{H^+} is proton current, Δp is the electrochemical proton motive force and $C_m H^+$ is the membrane conductance of protons [42, 43].

The series of reductive reactions of the protein complexes I–IV that comprise the ETC results in the accumulation of H^+ outside of the membrane. Through the ATP generating F1/F0 ATP synthase (Complex V), these protons return to the mitochondria, producing ATP in the process and concluding the ETC. The Δp is the overall force driving protons back into the mitochondrial matrix. It consists of the electrical or charge gradient, $\Delta\psi_m$, and chemical or concentration gradient, ΔpH , the difference between pH in the matrix and intermembrane space, which usually amounts to -0.5 up to -1 units (the mitochondrial matrix is alkaline) [44]. Thus, Δp can be calculated via the equation expressing proton electrochemical gradient, as follows (at $37^\circ C$) [43]:

$$\Delta p = \Delta\psi_m - 61 * \Delta pH \quad (6)$$

In physiological homeostatic conditions, $\Delta\psi_m$ amounts to 150 – 180 mV, and with ΔpH somewhere between -1 and -0.5 units, Δp falls in range 180 – 220 mV.

The above noted equation emphasises essential distinction, the probes described in this section are all related to $\Delta\psi_m$, evaluating the charge gradient across the IMM, but do not pertain to ΔpH . The list of fluorescent probes used to monitor the $\Delta\psi_m$ comprises of rhodamine (rhodamine 123—R123, tetramethylrhodamine methyl ester—TMRM and tetramethylrhodamine ethyl ester—TMRE), and cyanine derivatives (5,5',6,6'-tetrachloro 1,1',3,3'-tetramethylbenzimidazolyl carbocyanine iodide—JC-1; 3,3'-dihexyloxa carbocyanine iodide—DiOC6(3)). **Figure 10** depicts representatives of these two groups of compounds, both LCs, taking advantage of the compliance with the membrane passage described in Section 3 of this chapter and the charge gradient described above.

There are two experimental scenarios when the measurement of the $\Delta\psi_m$ is considered: first, when the real-time changes in $\Delta\psi_m$, as a response to some treatment, needs to be monitored. The great advantage of this experimental setup is the fact that the sample before treatment can serve as a baseline. Another scenario can be described as the evaluation of change in $\Delta\psi_m$ caused by a chronic experimental

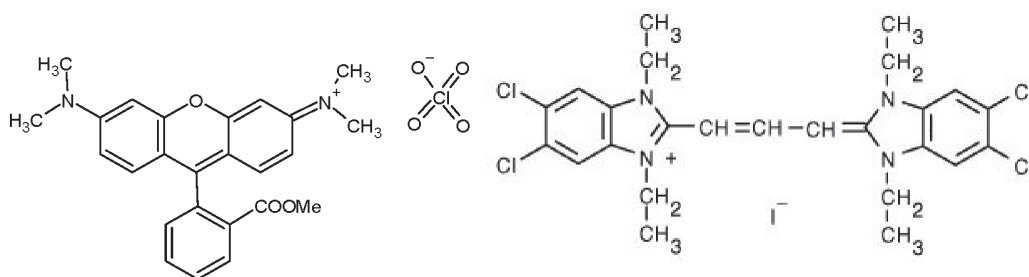


Figure 10.
TMRM and JC-1 structures.

treatment such as chronic exposure to a chemical, or gene manipulation. This methodology is usually implemented on the larger population of cells/mitochondria, showing a change on average. In this case, the baseline or control group has to be prepared from the non-treated sample. The choice of the probe depends on the experimental set-up. Further considerations include the mode of the usage and the choice of the readout methodology, which altogether impacts the selection of the probe. The probe can be used in turn-off (quenching) mode or turn-on fluorescence mode. For the quenching mode, high dye concentrations have to be used (up to several μM), so upon the uptake by mitochondria the autoquenching takes place, as the intramitochondrial concentration is such that the aggregation occurs, decreasing the fluorescence signal. After loading the mitochondria, the externally caused depolarisation, for example by treatment with carbonyl cyanide-p-trifluoromethoxy phenyl hydrazine (FCCP), will result in disaggregation and unquenching of the dye, increase of the fluorescent signal. Contrariwise, hyperpolarisation of mitochondria (oligomycin treatment) will result in higher accumulation of the probe and further quenching of the fluorescence emission. Quenching mode can be used only for the first type of scenario, where acute real-time changes in $\Delta\psi_m$ are observed [45]. Instead of the standard, proposed depolarisation or hyperpolarisation treatments, the investigated agent can be used to evaluate its effect on $\Delta\psi_m$.

In turn-on fluorescence mode, probe concentrations used are lower (up to 50 nM) to prevent the aggregation and the quenching of the fluorescence. Thus, more polarised mitochondria accumulate more probe and emit more fluorescence and the mitochondria with lower $\Delta\psi_m$ store lower concentrations of the probe and emit less fluorescence. In this mode, however, both experimental scenarios can be employed; acute changes can be implemented after the probe loading while chronic treatments should be performed before probe loading. There are several protocols published by research groups [46, 47] and the manufacturers/distributors of the probes disclose the protocols pertained to their specific probe. However, when using these probes, researchers must be aware of the detrimental effects that these probes can evoke. These effects can be caused by photodynamic generation of singlet oxygen or other reactive oxygen species or simply by ETC inhibition. **Table 1** shows the spectral characteristics and practical considerations needed to determine the optimal probe for the specific experiment [45].

When performing a $\Delta\psi_m$ evaluation experiment, regardless of the mode and experimental scenarios, all the influences that can affect the loading and fluorescence signal of the probe should be considered. As mentioned above, when acute real-time changes are measured (Scenario 1), the baseline can be the output before the change infliction. Therefore, special precautions should be considered in performing chronic scenario measurements. The probe concentration in mitochondria is affected by (a) probe concentration in the bath; (b) cell membrane potential; (c) mitochondrial size/mass (surface to volume ratio); (d) loading time and, of course, (e) $\Delta\psi_m$. Except for the measured $\Delta\psi_m$, all other factors should be controlled and should not change during measurement. Nevertheless, in a turn-on fluorescence mode, using lowest possible dye concentrations and leaving the probe in the bath during measurement (no wash-out step) should in general result in reproducible assessments of post-treatment $\Delta\psi_m$ across different samples, if all other above-mentioned factors are fixed or controlled.

5. pH probes

Considering that 80% of the Δp is due to $\Delta\psi_m$, researchers usually focus on measurement, control and investigation of $\Delta\psi_m$ and disregard the relatively small

Probe	Spectral characteristics	Experimental considerations
TMRM, TMRE Probes of choice for slow resolving acute study scenarios or measuring pre-existing $\Delta\psi_m$		<ul style="list-style-type: none">• TMRM shows lowest ETC inhibition [47]• Lowest possible conc. if used in turn-on mode < 30 nM; quenching mode use 50–100 nM• Fast mitochondria loading and equilibration• Both acute and chronic study scenarios
R-123 Best for fast resolving acute studies, turn-off mode		<ul style="list-style-type: none">• Preferably used in quenching mode (1–10 μM), monitoring acute changes in $\Delta\psi_m$ after loading and washing out the excess• Note: ETC inhibition slightly less than TMRE but more than TMRM
JC-1 Best for a qualitative distinction of the polarisation state (apoptosis studies, flow cytometry or microscopy)		<ul style="list-style-type: none">• Monomer and J-aggregated form of the probe exhibit different emission maxima (515 and 590 nm, relatively, see spectra), allowing dual colour ratiometric assessment of $\Delta\psi_m$• Best if loaded after exp. treatment and left in the bath during imaging to prevent redistribution of the probe• Note: aggregate formation can be affected by factors other than $\Delta\psi_m$, such as surface-to-volume ratios and H_2O_2. JC-1 likely requires longer equilibration times than reported
DiOC ₆ (3) Best for flow cytometry		<ul style="list-style-type: none">• Most widely used for flow cytometry studies• Should be used in very low concentrations (<1 nM) due to respiration toxicity [48]

Table 1.
Mitochondrial membrane potential probes, spectral characteristics and experimental considerations.

contribution of ΔpH . Thus, in standard physiological conditions, ΔpH accounts for 20% of the Δp , but when $\Delta \psi_m$ fluctuates for whatever reason, Δp remains constant due to the compensation by ΔpH . This compensation can extend to a full amount, and Δp can be maintained solely by ΔpH contribution [49] and *vice versa*—when the chemical gradient of protons is diminished by extrinsic addition of ionophore (nigericin), Δp is maintained by $\Delta \psi_m$ only [50]. Hence, to fully understand and evaluate the mitochondrial state, both contributions must be considered. In consort with the proton motive force contribution, ΔpH regulates mitochondrial calcium, sodium and potassium fluxes as $Ca^{2+}-H^+$ [51]; Na^+-H^+ and K^+-H^+ [52] exchange transporters depend on ΔpH [53]. The $Pi-H^+$ phosphate cotransporter, responsible for the importation of phosphate ion for the ATP synthesis, also relies on ΔpH [54]. The uncoupling proteins, H^+ channels that uncouple the oxidative phosphorylation from the ATP synthesis and the permeability transition pores that initiate the cell death by opening their large ion channels, allowing nonselective influx across the IMM, depend on both, ΔpH and $\Delta \psi_m$.

So, the chemical proton gradient, ΔpH , is a sort of an underappreciated smaller associate of the electrical, charge gradient $\Delta \psi_m$. However, the reason why this contribution to the proton motive force has been ‘neglected’ is not only the scale of impact but also more challenging measurement. The search for the optimal pH sensor for mitochondria is an ongoing task. The ideal sensor should efficiently target mitochondria, exhibit no toxicity or phototoxicity, display wide dynamic range with the prompt and reversible response to changes in pH and show slightly alkaline pK_a , as the mitochondrial matrix pH is in 7.5–8.5 range. Furthermore, they should be ratiometric to allow compensation for the different cell morphologies and sensor uptake. Historically, mitochondrial pH was measured using radioactively tagged weak acids and bases [55], but the introduction of fluorescent pH-sensitive probes allowed more detailed measurements, with spatial, single-cell resolution [56, 57]. These pH sensors are based on fluorescein structure and are not mitochondria targeted. Thus, if used for a whole cell measurement, cells should also be loaded with mitochondrial morphology probes to distinguish the fluorescence pH-related signal from mitochondrial and cytosolic areas. The photodynamic properties of such sensors are also a concern, as they usually produce ROS upon light excitation. The main representative is carboxy SNARF 1 (**Figure 11**), the cell permeant, pH-sensitive dye, with pK_a of 7.5 and consequently suitable for measuring the pH in the range 7–8. The fluorescence emission can be measured ratiometrically using emission bands at 580 and 640 nm. Visually, upon the increase of the pH, the emission shifts from yellow-orange towards deep red fluorescence. The fluorescence

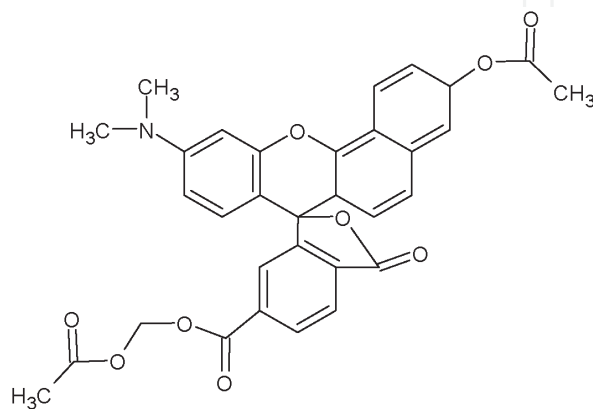


Figure 11.
Spiro[7H-benzo[c]xanthene-7,1'(3H)-isobenzofuran]-ar'-carboxylic acid, 3-(acetyloxy)-10-(dimethylamino)-3'-oxo-, (acetyloxy)methyl ester or shorter 6-carboxy SNARF-1, Acetoxymethylester, Acetat.

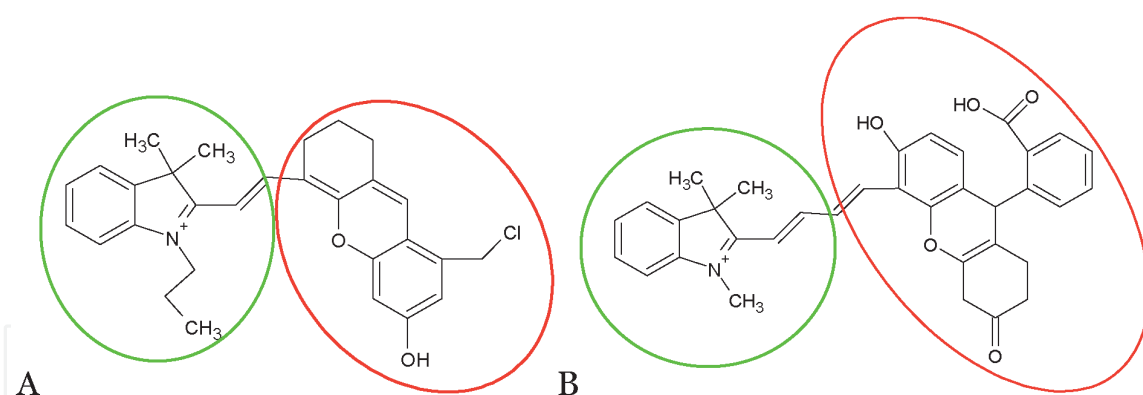


Figure 12.
(A) HXPI-Cl mitochondrial pH sensor [60], (B) FDI mitochondrial pH sensor [61].

measurements can be performed using flow cytometer, fluorescence plate reader or fluorescence microscopy.

Targeting mitochondria is not a problem for engineered protein constructs bearing MTS. Considering that the fluorescence properties of FPs naturally depend on the protonation state of its chromophore, located inside the β -barrel of the protein, they can be transformed into pH sensors [58, 59].

As the interest for mitochondrial pH measurement gained momentum [44], so did the pursuit for new and improved pH sensors that would efficiently target mitochondria. There are more new sensors synthesised and published [60, 61] but the general idea of their design is similar. They usually consist of a pH-sensitive moiety (red circled in **Figure 12**) unsaturated (di)alkene bridge and an indole quaternary ammonium moiety, LC, responsible for mitochondria targeting (green circled in **Figure 12**). The (di)alkene bridge affords ratiometric measurements by broadening the absorption and emission spectra.

6. Redox sensors

ROS were mentioned in this chapter more than once, in relation to the phototoxic probes that invoke production of singlet oxygen and ROS, and as a by-product of mitochondrial metabolism. Mitochondria are the major ROS producers in the cell, being a part of physiological or pathological processes [62, 63]. The ROS that is first produced in mitochondria is superoxide anion (O_2^-), a product of mitochondrial respiratory chain. However, the main signalling molecule is H_2O_2 generated by manganese superoxide dismutase, which is abundantly concentrated in the mitochondrial matrix and quickly converts O_2^- to H_2O_2 . Due to its short life and poor diffusion, O_2^- is not a prominent signalling molecule. When respiratory complex III generates O_2^- and releases it into the intermembrane space, it can diffuse to the cytosol or gets converted to H_2O_2 by the Cu,Zn-superoxide dismutase, which is present there [64]. Mitochondrial redox signalling mechanism also involves the regulation of the concentration of formed H_2O_2 in the matrix, via peroxiredoxins (Prx3 and Prx5) and glutathione peroxidase 1 (Gpx1) [65]. Peroxiredoxins employ mitochondrial thioredoxin 2 reduction system, while Gpx1 engage glutathione for H_2O_2 reduction. Nitric oxide (NO) is another ROS that modulates mitochondrial function. It is generated by NO synthase, once it accumulates in the matrix [66]. The ability to affect modification of the protein, causing reversible alteration of its functionality, renders H_2O_2 and NO efficient biological messengers. Modification of a thiol on a cysteine residue by H_2O_2 oxidation into a disulphide, changing the activity of the protein, is an example of a signalling cascade. Once the levels of the redox signal return to the baseline

concentrations, the modification is reversed, and the protein regains its function [67]. Numerous reviews describe the redox signalling and redox pathologies in mitochondria, and further explanation would fall outside of the scope of this chapter.

The mitochondrial fluorescent redox sensors are listed in **Table 2** [86]. They again use the same two strategies for mitochondrial targeting, LCs or MTSs.

The different principles of fluorescence response provoked by ROS are shown in the series of figures below. ROS can instigate the cleavage of the masking groups

Name	Targeting group	Ex/Em (nm)	Selectivity	Measuring mode
Lipophilic cations				
MitoSOX [68, 69]	Triphenylphosphonium ion (TPP)	510/580	O_2^- , OH $^\cdot$, ONOO $^-$	Turn-on, irreversible
MitoPY1 [70]		515/543	H $_2$ O $_2$, ONOO $^-$, OCl $^-$	Turn-on, irreversible
SSH-Mito [71]		338/462 and 545	Thiols	Emission ratiometric (F545/F462 increase), irreversible
NpFR2 [72]	rhodamine	488/545	Total ROS	Turn-on, reversible
MitoAR/ MitoHR [73]		553/574	OH $^\cdot$, ONOO $^-$, OCl $^-$	Turn-on, irreversible
RhoSS [74]		500/530	Thiols	Turn-on, irreversible
FRR2 [75]		460 and 550/590	Total ROS	Excitation ratiometric (F550/F460 increase), reversible
Cy-O-EB [76]	cyanine	768/794	H $_2$ O $_2$	Turn-on, reversible
pep3-NP1 [77]	styryl	455(442)/555 (646)	H $_2$ O $_2$	Emission ratiometric (F646/F555 increase), irreversible
Fluorescent protein constructs carrying MTS				
roGFP1 and roGFP2 [78, 79]	Pyruvate dehydrogenase (COX4)	395 and 475 (GFP1) 490 (GFP2)/508	General redox status	Excitation ratiometric (F395/F475 (F490) increase), reversible
HyPer [80]	Two copies human COX8	420 and 500/516	H $_2$ O $_2$	Excitation ratiometric (F500/F420 increase), reversible
rxYFP [81]	COX4	512/523	General redox status	Turn-off upon oxidation, reversible
Grx1-roGFP2 [82]	Non-human ATP synthase prot 9	395 and 488/508	GSH/GSSG redox couple	Excitation ratiometric (F395/F488 increase), reversible
Orp1-roGFP2 [83]	Human COX8	395 and 488/508	H $_2$ O $_2$	Excitation ratiometric (F395/F488 increase), reversible
HyPerRed [84]	Two copies human COX8	560/605	H $_2$ O $_2$	Turn-on, reversible
Sulphonyl fluorescein [85]	Human COX8	495/519	O_2^-	Turn-on, irreversible

OH $^\cdot$, hydroxyl radical.

Table 2.
Mitochondrial redox sensors.

(**Figures 13 and 14**), quenching moieties (**Figure 15**), but also transform the sensor structure into a rigid form that exhibits high fluorescence (**Figure 16**) and allow fluorescence resonance energy transfer (FRET) pairing (**Figure 17**).

Sulphonyl fluorescein, the small molecule sensor, targets mitochondria with 25 amino acid-long MTS. Upon reaction with superoxide anion, fluorescein is released (**Figure 18**). This confirms that MTSs can also facilitate the transport of small molecules to the mitochondria.

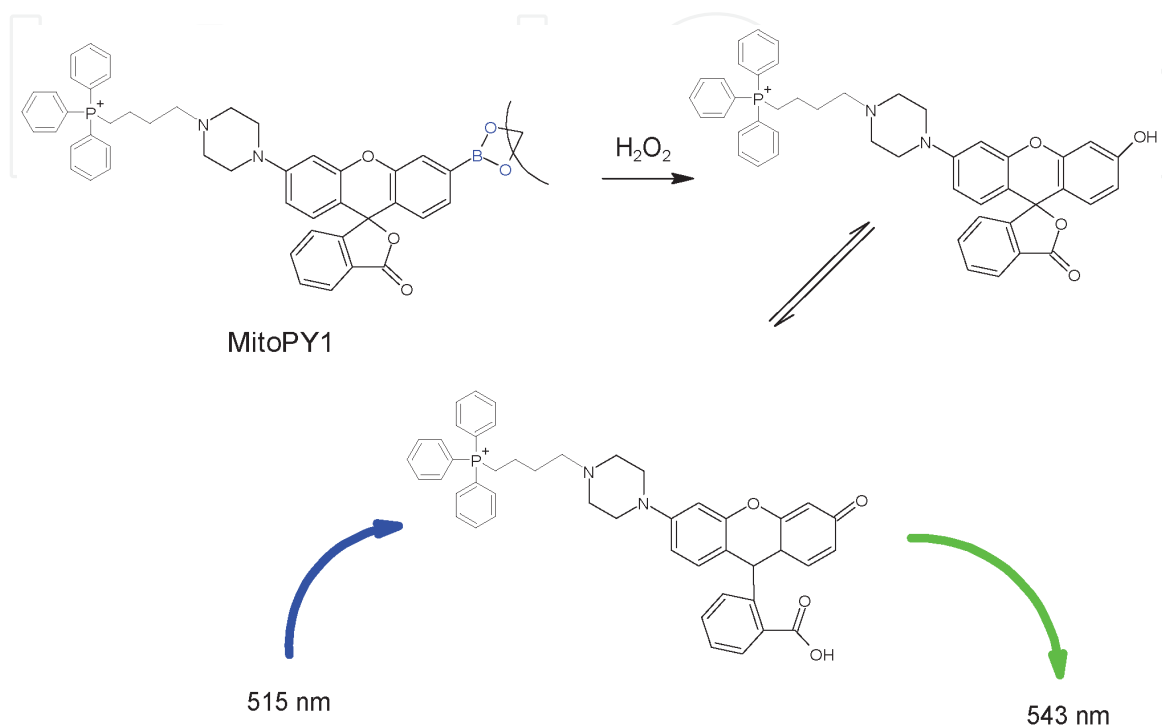


Figure 13.

MitoPy1 redox sensor, upon reaction with H_2O_2 or peroxynitrite ($ONOO^-$), the boronate masking group is cleaved, initiating tautomerisation and subsequent fluorescence response. Since the boronate cleavage is not reversible, the fluorescence signal is also irreversibly turned on.

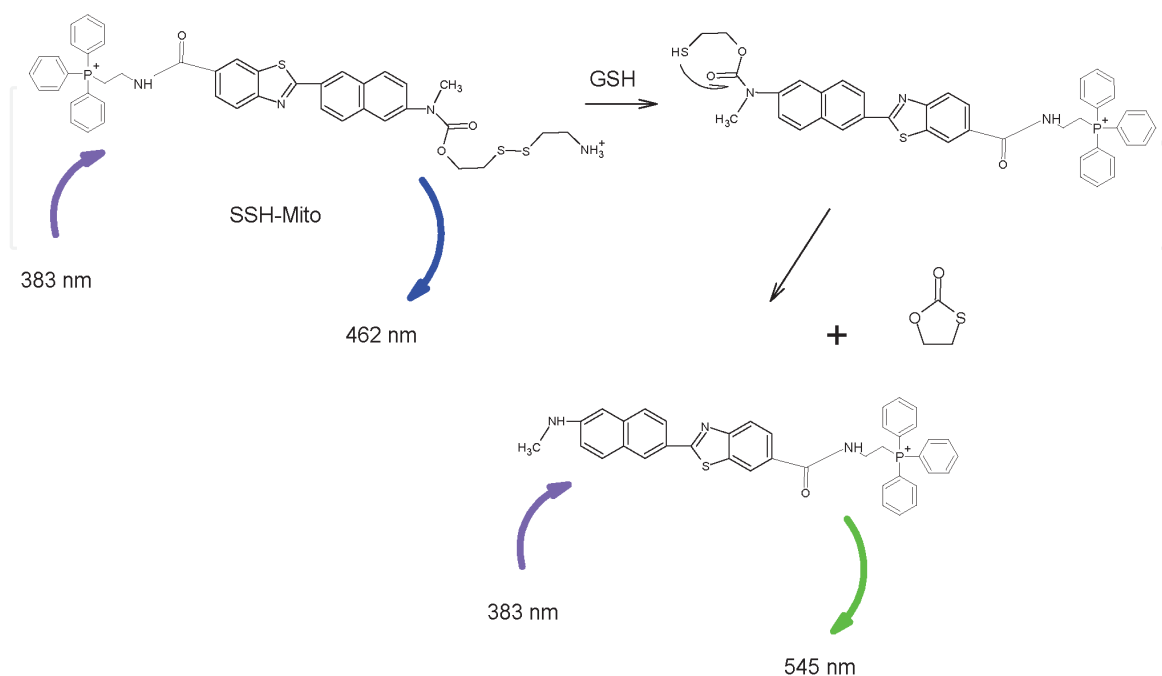


Figure 14.

SSH-Mito with a redox-sensitive disulphide bond, reduction of this bond instigates reaction sequence that results in a redshift of the fluorescence emission.

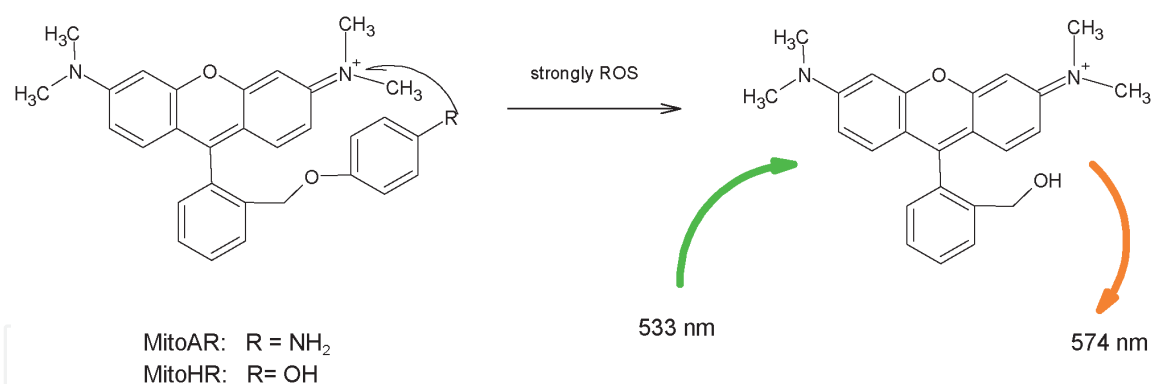


Figure 15.
The fluorescence quencher is cleaved by highly reactive oxygen species from the rhodamine derivatives MitoAR and MitoHR.

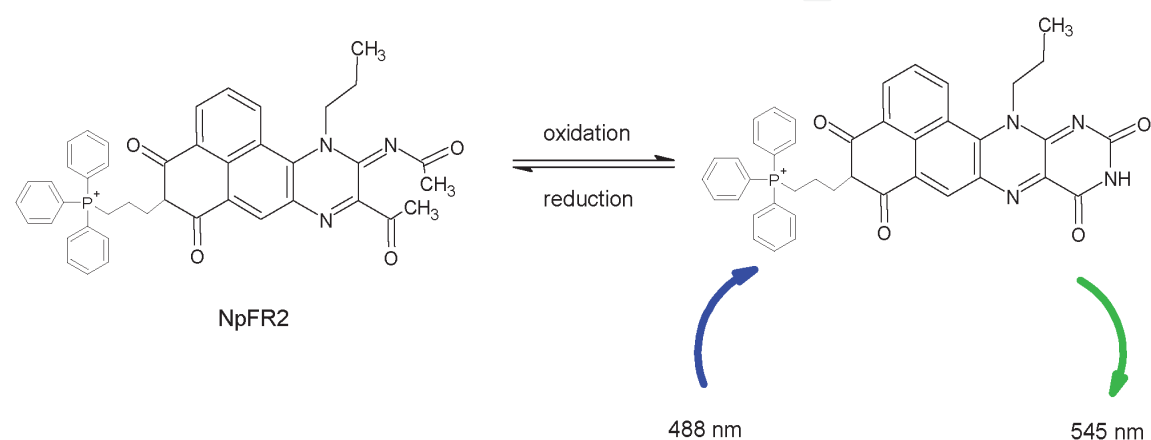


Figure 16.
NpFR2 upon oxidation is reversibly transformed from a flexible bent structure to a rigid highly fluorescent one.

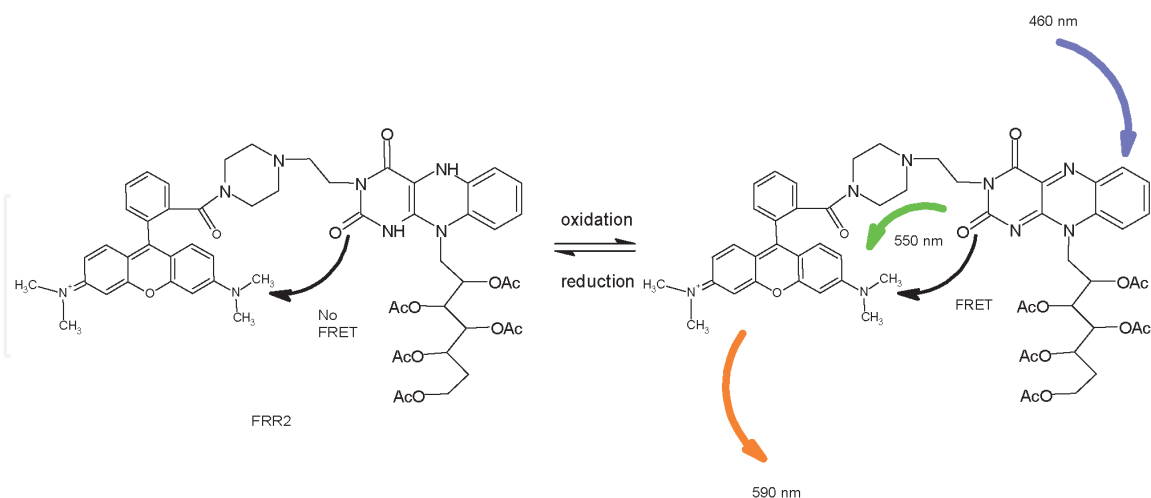
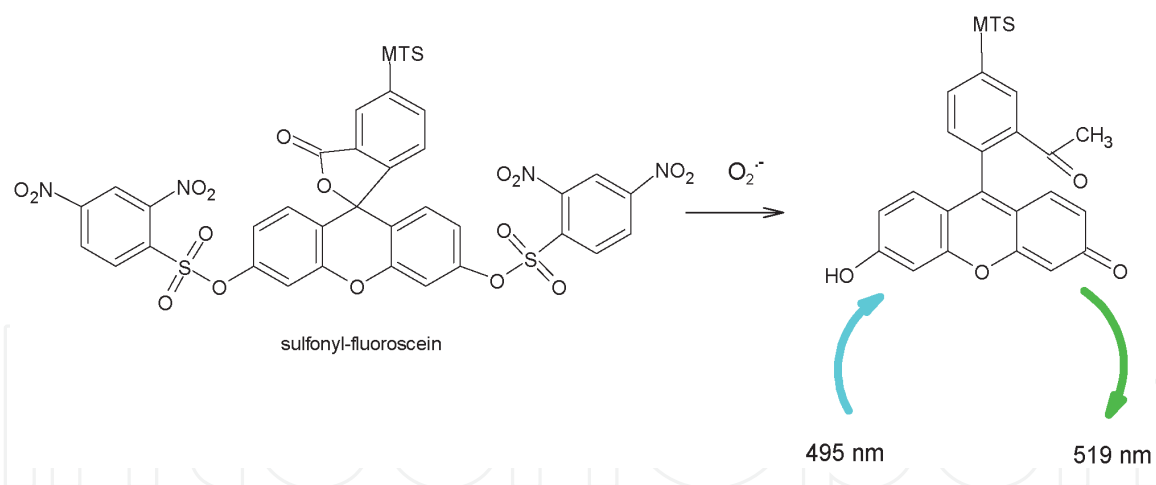


Figure 17.
The FRR2 sensor reports on ROS presence by FRET pairing, with riboflavin as a FRET donor and rhodamine as an acceptor.

7. (Instead of) Conclusion

The main types of fluorescent probes and sensors are described in the above sections. The new ones should report on characteristics that are not yet covered or have dual signalling capabilities. The fluorescent temperature sensor was mentioned in the abstract of this chapter. The sensor, MitoThermo Yellow, is, in fact, a

**Figure 18.**

Sulphonyl fluorescein, small molecule fluorescent sensor, targeting mitochondria through MTS.

rhodamine analogue [87, 88]. The pentamethine analogue Mito-V reports on intramitochondrial viscosity [89]. There are others, that were not yet mentioned. For example, fluorescent ion probes like Ca^{2+} , Na^{+} and K^{+} sensors are important and frequently used to evaluate mitochondrial physiology. However, they are not actually mitochondria targeted, so the experimental set-up includes colocalisation staining with one of the mitochondrial morphology probes (**Figure 4(A)**). There is also a whole field of mitochondria targeted fluorescent methodology that was not covered, fluorescence-based immunohistochemistry (immunofluorescence) because it exceeds the scope of this chapter. Mitochondrial physiology and dysfunction are always going to be a topic of great interest. The search for the new dyes, sensors and probes will probably be driven by the technological developments in the detection of the signalling molecules, membrane potentials and morphological characteristics of mitochondria. Regarding fluorescence detection, ‘the future’ is already here, the technology allowing the resolution to go beyond the diffraction limit is already in use. Stimulated emission depletion microscopy (STED), proposed in 1994 [90], brought its inventors Nobel Prize in chemistry 20 years later and the first ready-made STED microscopes are coming to the market 25 years later. Mitochondrial STED imaging is still a novelty, but the STED microscopy studies on mitochondria are growing in numbers [91, 92]. The desired characteristics for STED dyes are not that different from characteristics of standard fluorescence probes. Brightness, low toxicity/phototoxicity and efficient targeting, those are features needed for all types of fluorescent imaging. Photostability is also a requirement for all types of imaging. Still, for STED microscopy, due to high laser beam energies involved, the dye has to be almost entirely resistant to photodegradation. Another difference is that for STED, excitation/emission should be in the far-red, near-infrared range. Having tunable absorption/emission properties and relatively high photostability, previously mentioned cyanine dyes are excellent candidates for this type of imaging. In whatever direction the technology takes the research, targeting mitochondria will probably always depend on MTSs or LCs. However, with this previously unthinkable resolutions, the spatial positioning of a mitochondrial targeting moiety and a fluorophore attached to it does not necessarily have to be the same. The quest for new mitochondrial fluorescent probes is ongoing.

Acknowledgements

I would like to extend my gratitude to Dr. Marijana Radić Stojković and Dr. Lidija-Marija Tumir from Ruđer Bošković Institute for their help with the text.

Thanks

Greatest thanks to my family, Nina, Hana and Marko, they are my inspiration always. However, this time their patience was tested more thoroughly as this chapter was written during the quarantine due to the Covid-19 pandemic.

IntechOpen


IntechOpen

Author details

Ivo Crnolatac
Ruđer Bošković Institute, Zagreb, Croatia

*Address all correspondence to: icrnolat@irb.hr

IntechOpen

© 2020 The Author(s). Licensee IntechOpen. Distributed under the terms of the Creative Commons Attribution - NonCommercial 4.0 License (<https://creativecommons.org/licenses/by-nc/4.0/>), which permits use, distribution and reproduction for non-commercial purposes, provided the original is properly cited. 

References

- [1] Susin SA, Zamzami N, Kroemer G. Mitochondria as regulators of apoptosis: Doubt no more. *Biochimica et Biophysica Acta*. 1998;**1366**:151-165
- [2] Bhola PD, Letai A. Mitochondria—Judges and executioners of cell death sentences. *Molecular Cell*. 2016;**61**: 695-704. DOI: 10.1016/j.molcel.2016.02.019
- [3] Lenaz G. Role of mitochondria in oxidative stress and ageing. *Biochimica et Biophysica Acta (BBA)—Bioenergetics*. 1998;**1366**:53-67. DOI: 10.1016/S0005-2728(98)00120-0
- [4] Sun N, Youle RJ, Finkel T. The mitochondrial basis of aging. *Molecular Cell*. 2016;**61**:654-666. DOI: 10.1016/j.molcel.2016.01.028
- [5] Ichas F, Mazat JP. From calcium signaling to cell death: Two conformations for the mitochondrial permeability transition pore. Switching from low-to high-conductance state. *Biochimica et Biophysica Acta*. 1998;**1366**:33-50
- [6] Bravo-Sagua R, Parra V, López-Crisosto C, Díaz P, Quest AFG, Lavandero S. Calcium transport and signaling in mitochondria. In: Terjung R, editor. *Comprehensive Physiology*. Hoboken, NJ, USA: John Wiley & Sons, Inc.; 2017. pp. 623-634. DOI: 10.1002/cphy.c160013
- [7] Mitra K, Wunder C, Roysam B, Lin G, Lippincott-Schwartz J. A hyperfused mitochondrial state achieved at G1-S regulates cyclin E buildup and entry into S phase. *Proceedings of the National Academy of Sciences*. 2009;**106**:11960-11965. DOI: 10.1073/pnas.0904875106
- [8] Salazar-Roa M, Malumbres M. Fueling the cell division cycle. *Trends in Cell Biology*. 2017;**27**:69-81. DOI: 10.1016/j.tcb.2016.08.009
- [9] Bonilla E, Tanji K, Hirano M, Vu TH, DiMauro S, Schon EA. Mitochondrial involvement in Alzheimer's disease. *Biochimica et Biophysica Acta (BBA)—Bioenergetics*. 1999;**1410**:171-182. DOI: 10.1016/S0005-2728(98)00165-0
- [10] Schapira AHV. Mitochondrial involvement in Parkinson's disease, Huntington's disease, hereditary spastic paraplegia and Friedreich's ataxia. *Biochimica et Biophysica Acta (BBA)—Bioenergetics*. 1999;**1410**:159-170. DOI: 10.1016/S0005-2728(98)00164-9
- [11] Wallace DC. Mitochondria and cancer. *Nature Reviews. Cancer*. 2012; **12**:685-698. DOI: 10.1038/nrc3365
- [12] Modica-Napolitano JS, Kulawiec M, Singh KK. Mitochondria and human cancer. *Current Molecular Medicine*. 2007;**7**:121-131. DOI: 10.2174/156652407779940495
- [13] Singh KK, Kulawiec M, Still I, Desouki MM, Geradts J, Matsui S-I. Inter-genomic cross talk between mitochondria and the nucleus plays an important role in tumorigenesis. *Gene*. 2005;**354**:140-146. DOI: 10.1016/j.gene.2005.03.027
- [14] Lee S, Kim S, Sun X, Lee J-H, Cho H. Cell cycle-dependent mitochondrial biogenesis and dynamics in mammalian cells. *Biochemical and Biophysical Research Communications*. 2007;**357**: 111-117. DOI: 10.1016/j.bbrc.2007.03.091
- [15] Gray MW, Burger G, Lang BF. Mitochondrial evolution. *Science*. 1999; **283**:1476-1481. DOI: 10.1126/science.283.5407.1476
- [16] D'Souza AR, Minczuk M. Mitochondrial transcription and translation: Overview. *Essays in Biochemistry*. 2018;**62**:309-320. DOI: 10.1042/EBC20170102

- [17] Ott M, Herrmann JM. Co-translational membrane insertion of mitochondrially encoded proteins. *Biochimica et Biophysica Acta*. 2010; **1803**:767-775. DOI: 10.1016/j.bbamcr.2009.11.010
- [18] Schmidt O, Pfanner N, Meisinger C. Mitochondrial protein import: From proteomics to functional mechanisms. *Nature Reviews. Molecular Cell Biology*. 2010; **11**:655-667. DOI: 10.1038/nrm2959
- [19] PDHA1. Pyruvate Dehydrogenase E1 Component Subunit Alpha, Somatic Form, Mitochondrial Precursor—Homo Sapiens (Human). PDHA1 Gene & Protein. Available from: <https://www.uniprot.org/uniprot/P08559>
- [20] COX8A. Cytochrome C Oxidase Subunit 8A, Mitochondrial Precursor—Homo Sapiens (Human)—COX8A Gene & Protein. Available from: <https://www.uniprot.org/uniprot/P10176>
- [21] CellLight™ Mitochondria-GFP, BacMam 2.0. Available from: <http://www.thermofisher.com/order/catalog/product/C10600>
- [22] Mitochondria Cyto-Tracer™, pCT-Mito-GFP (MSCV) | System Biosciences. Available from: <https://systembio.com/shop/pct-mito-gfp-pmscv-mitochondria-cox8-tag/>
- [23] Addgene: Fluorescent Protein Guide: Subcellular Localization. Available from: <https://www.addgene.org/fluorescent-proteins/localization/>
- [24] Sirk DP, Zhu Z, Wadia JS, Mills LR. Flow cytometry and GFP: A novel assay for measuring the import and turnover of nuclear-encoded mitochondrial proteins in live PC12 cells. *Cytometry. Part A*. 2003; **56**:15-22. DOI: 10.1002/cyto.a.10084
- [25] Friedman JR, Lackner LL, West M, DiBenedetto JR, Nunnari J, Voeltz GK. ER tubules mark sites of mitochondrial division. *Science*. 2011; **334**:358-362. DOI: 10.1126/science.1207385
- [26] Crnolatac I, Tumir L-M, Lesev NY, Vasilev AA, Deligeorgiev TG, Mišković K, et al. Probing the structural properties of DNA/RNA grooves by sterically restricted phosphonium dyes; screening of dye cell toxicity and uptake. *ChemMedChem*. 2013; **8**: 1093-1103. DOI: 10.1002/cmdc.201300085
- [27] Organelle Stains Products, Cell Stains. Thermo Fisher Scientific. Available from: <https://www.thermofisher.com/search/results?query=organelle+stains&persona=Catalog&navId=16601&refinementAction=true&focusarea=Suchen+in+Alle>
- [28] MitoSpy™. Mitochondrial Probes. Available from: https://www.biolegend.com/en-us/mitospy?gclid=CjwKCAjw7e_0BRB7EiwAlH-goFmlW06US19mt9eRXmaSL4BYT_z527E2E-icloP1YmYiWjUq_AvOvhoCemEQAvD_BwE
- [29] Šarić A, Crnolatac I, Bouillaud F, Sobocanec S, Mikecin A-M, Mačak Šafranko Ž, et al. Non-toxic fluorescent phosphonium probes to detect mitochondrial potential. *Methods and Applications in Fluorescence*. 2017; **5**: 015007. DOI: 10.1088/2050-6120/aa5e64
- [30] Kurutos A, Orehovec I, Tomašić Paić A, Crnolatac I, Horvat L, Gadjev N, et al. New series of non-toxic DNA intercalators, mitochondria targeting fluorescent dyes. *Dyes and Pigments*. 2017; **148**:452-459. DOI: 10.1016/j.dyepig.2017.09.049
- [31] Kurutos A, Orehovec I, Saftić D, Horvat L, Crnolatac I, Piantanida I, et al. Cell penetrating, mitochondria targeting multiply charged DABCO-cyanine dyes. *Dyes and Pigments*. 2018; **158**:517-525. DOI: 10.1016/j.dyepig.2018.05.035
- [32] Manders EMM, Verbeek FJ, Aten JA. Measurement of co-localization

- of objects in dual-colour confocal images. *Journal of Microscopy*. 1993; **169**:375-382. DOI: 10.1111/j.1365-2818.1993.tb03313.x
- [33] Schneider CA, Rasband WS, Eliceiri KW. NIH image to ImageJ: 25 years of image analysis. *Nature Methods*. 2012;**9**:671-675. DOI: 10.1038/nmeth.2089
- [34] Adler J, Pagakis SN, Parmryd I. Replicate-based noise corrected correlation for accurate measurements of colocalization. *Journal of Microscopy*. 2008;**230**:121-133. DOI: 10.1111/j.1365-2818.2008.01967.x
- [35] Demchenko AP. Photobleaching of organic fluorophores: Quantitative characterization, mechanisms, protection. *Methods and Applications in Fluorescence*. 2020;**8**:022001. DOI: 10.1088/2050-6120/ab7365
- [36] Armitage BA. Cyanine dye–DNA interactions: Intercalation, groove binding, and aggregation. In: Waring MJ, Chaires JB, editors. *DNA Binders and Related Subjects*. Topics in Current Chemistry. Berlin, Heidelberg: Springer; 2005. pp. 55-76. DOI: 10.1007/b100442
- [37] Honig BH, Hubbell WL, Flewelling RF. Electrostatic interactions in membranes and proteins. *Annual Review of Biophysics and Biophysical Chemistry*. 1986;**15**:163-193. DOI: 10.1146/annurev.bb.15.060186.001115
- [38] Flewelling RF, Hubbell WL. The membrane dipole potential in a total membrane potential model. Applications to hydrophobic ion interactions with membranes. *Biophysical Journal*. 1986;**49**:541-552. DOI: 10.1016/S0006-3495(86)83664-5
- [39] Ross MF, Kelso GF, Blaikie FH, James AM, Cochemé HM, Filipovska A, et al. Lipophilic triphenylphosphonium cations as tools in mitochondrial bioenergetics and free radical biology. *Biochemistry (Moscow)*. 2005;**70**: 222-230. DOI: 10.1007/s10541-005-0104-5
- [40] Ketterer B, Neumcke B, Läger P. Transport mechanism of hydrophobic ions through lipid bilayer membranes. *Journal of Membrane Biology*. 1971;**5**: 225-245. DOI: 10.1007/BF01870551
- [41] Alberts B, Johnson A, Lewis J, Raff M, Roberts K, Walter P. *Molecular Biology of the Cell*. 4th ed. New York, USA: Garland Science; 2002
- [42] Nicholls DG, Ward MW. Mitochondrial membrane potential and neuronal glutamate excitotoxicity: Mortality and millivolts. *Trends in Neurosciences*. 2000;**23**:166-174. DOI: 10.1016/s0166-2236(99)01534-9
- [43] David NG, Ferguson SJ. *Bioenergetics*. 4th ed. Amsterdam: Academic Press; 2013
- [44] Santo-Domingo J, Demaurex N. The renaissance of mitochondrial pH. *The Journal of General Physiology*. 2012;**139**: 415-423. DOI: 10.1085/jgp.201110767
- [45] Perry SW, Norman JP, Barbieri J, Brown EB, Gelbard HA. Mitochondrial membrane potential probes and the proton gradient: A practical usage guide. *BioTechniques*. 2011;**50**:98-115. DOI: 10.2144/000113610
- [46] Chazotte B. Labeling mitochondria with JC-1. *Cold Spring Harbor Protocols*. 2011;**2011**. DOI: 10.1101/pdb.prot065490
- [47] Scaduto RC, Grotyohann LW. Measurement of mitochondrial membrane potential using fluorescent rhodamine derivatives. *Biophysical Journal*. 1999;**76**:469-477
- [48] Rottenberg H, Wu S. Quantitative assay by flow cytometry of the mitochondrial membrane potential in

- p>intact cells.
- Biochimica et Biophysica Acta*
- . 1998;
- 1404**
- :393-404. DOI: 10.1016/s0167-4889(98)00088-3
- [49] Nicholls DG. Commentary on: 'Old and new data, new issues: The mitochondrial $\Delta\psi$ ' by H. Tedeschi. *Biochimica et Biophysica Acta (BBA)—Bioenergetics*. 2005;**1710**:63-65. DOI: 10.1016/j.bbabi.2005.09.002
- [50] Lambert AJ, Brand MD. Superoxide production by NADH:ubiquinone oxidoreductase (complex I) depends on the pH gradient across the mitochondrial inner membrane. *The Biochemical Journal*. 2004;**382**:511-517. DOI: 10.1042/BJ20040485
- [51] Jiang D, Zhao L, Clapham DE. Genome-wide RNAi screen identifies Letm1 as a mitochondrial $\text{Ca}^{2+}/\text{H}^{+}$ antiporter. *Science*. 2009;**326**:144-147. DOI: 10.1126/science.1175145
- [52] Nowikovsky K, Froschauer EM, Zsurka G, Samaj J, Reipert S, Kolisek M, et al. The LETM1/YOL027 gene family encodes a factor of the mitochondrial K^{+} homeostasis with a potential role in the wolf-Hirschhorn syndrome. *The Journal of Biological Chemistry*. 2004;**279**:30307-30315. DOI: 10.1074/jbc.M403607200
- [53] Bernardi P. Mitochondrial transport of cations: Channels, exchangers, and permeability transition. *Physiological Reviews*. 1999;**79**:1127-1155. DOI: 10.1152/physrev.1999.79.4.1127
- [54] Palmieri F. The mitochondrial transporter family (SLC25): Physiological and pathological implications. *Pflügers Archiv*. 2004;**447**:689-709. DOI: 10.1007/s00424-003-1099-7
- [55] Hoek JB, Nicholls DG, Williamson JR. Determination of the mitochondrial protonmotive force in isolated hepatocytes. *The Journal of Biological Chemistry*. 1980;**255**:1458-1464
- [56] Lemasters JJ, Chacon E, Ohata H, Harper IS, Nieminen AL, Tesfai SA, et al. Measurement of electrical potential, pH, and free calcium ion concentration in mitochondria of living cells by laser scanning confocal microscopy. *Methods in Enzymology*. 1995;**260**:428-444. DOI: 10.1016/0076-6879(95)60156-2
- [57] SNARF pH Indicators. Available from: <http://tools.thermofisher.com/content/sfs/manuals/mp01270.pdf>
- [58] Kneen M, Farinas J, Li Y, Verkman AS. Green fluorescent protein as a noninvasive intracellular pH indicator. *Biophysical Journal*. 1998;**74**:1591-1599
- [59] Abad MFC, Di Benedetto G, Magalhães PJ, Filippin L, Pozzan T. Mitochondrial pH monitored by a new engineered green fluorescent protein mutant. *The Journal of Biological Chemistry*. 2004;**279**:11521-11529. DOI: 10.1074/jbc.M306766200
- [60] Li X, Hu Y, Li X, Ma H. Mitochondria-immobilized near-infrared ratiometric fluorescent pH probe to evaluate cellular mitophagy. *Analytical Chemistry*. 2019;**91**:11409-11416. DOI: 10.1021/acs.analchem.9b02782
- [61] Li G, Zhang B, Song X, Xia Y, Yu H, Zhang X, et al. Ratiometric imaging of mitochondrial pH in living cells with a colorimetric fluorescent probe based on fluorescein derivative. *Sensors and Actuators B: Chemical*. 2017;**253**:58-68. DOI: 10.1016/j.snb.2017.06.065
- [62] Murphy MP. How mitochondria produce reactive oxygen species. *The Biochemical Journal*. 2009;**417**:1-13. DOI: 10.1042/BJ20081386
- [63] Balaban RS, Nemoto S, Finkel T. Mitochondria, oxidants, and aging. *Cell*. 2005;**120**:483-495. DOI: 10.1016/j.cell.2005.02.001
- [64] Okado-Matsumoto A, Fridovich I. Subcellular distribution of superoxide

- dismutases (SOD) in rat liver: Cu,Zn-SOD in mitochondria. *The Journal of Biological Chemistry*. 2001;**276**: 38388-38393. DOI: 10.1074/jbc.M105395200
- [65] Cox AG, Winterbourn CC, Hampton MB. Mitochondrial peroxiredoxin involvement in antioxidant defence and redox signalling. *The Biochemical Journal*. 2009;**425**: 313-325. DOI: 10.1042/BJ20091541
- [66] Moncada S, Erusalimsky JD. Does nitric oxide modulate mitochondrial energy generation and apoptosis? *Nature Reviews. Molecular Cell Biology*. 2002;**3**:214-220. DOI: 10.1038/nrm762
- [67] Eaton P. Protein thiol oxidation in health and disease: Techniques for measuring disulfides and related modifications in complex protein mixtures. *Free Radical Biology and Medicine*. 2006;**40**:1889-1899. DOI: 10.1016/j.freeradbiomed.2005.12.037
- [68] Zielonka J, Kalyanaraman B. Hydroethidine- and MitoSOX-derived red fluorescence is not a reliable indicator of intracellular superoxide formation: Another inconvenient truth. *Free Radical Biology and Medicine*. 2010;**48**:983-1001. DOI: 10.1016/j.freeradbiomed.2010.01.028
- [69] Robinson KM, Janes MS, Beckman JS. The selective detection of mitochondrial superoxide by live cell imaging. *Nature Protocols*. 2008;**3**: 941-947. DOI: 10.1038/nprot.2008.56
- [70] Dickinson BC, Chang CJ. A targetable fluorescent probe for imaging hydrogen peroxide in the mitochondria of living cells. *Journal of the American Chemical Society*. 2008;**130**:9638-9639. DOI: 10.1021/ja802355u
- [71] Lim CS, Masanta G, Kim HJ, Han JH, Kim HM, Cho BR. Ratiometric detection of mitochondrial thiols with a two-photon fluorescent probe. *Journal of the American Chemical Society*. 2011;**133**:11132-11135. DOI: 10.1021/ja205081s
- [72] Kaur A, Brigden KWL, Cashman TF, Fraser ST, New EJ. Mitochondrially targeted redox probe reveals the variations in oxidative capacity of the haematopoietic cells. *Organic & Biomolecular Chemistry*. 2015;**13**: 6686-6689. DOI: 10.1039/C5OB00928F
- [73] Koide Y, Urano Y, Kenmoku S, Kojima H, Nagano T. Design and synthesis of fluorescent probes for selective detection of highly reactive oxygen species in mitochondria of living cells. *Journal of the American Chemical Society*. 2007;**129**:10324-10325. DOI: 10.1021/ja073220m
- [74] Pires MM, Chmielewski J. Fluorescence imaging of cellular glutathione using a latent rhodamine. *Organic Letters*. 2008;**10**:837-840. DOI: 10.1021/ol702769n
- [75] Kaur A, Jankowska K, Pilgrim C, Fraser ST, New EJ. Studies of hematopoietic cell differentiation with a ratiometric and reversible sensor of mitochondrial reactive oxygen species. *Antioxidants & Redox Signaling*. 2016;**24**:667-679. DOI: 10.1089/ars.2015.6495
- [76] Xu K, Qiang M, Gao W, Su R, Li N, Gao Y, et al. A near-infrared reversible fluorescent probe for real-time imaging of redox status changes in vivo. *Chemical Science*. 2013;**4**:1079-1086. DOI: 10.1039/C2SC22076H
- [77] Wen Y, Liu K, Yang H, Liu Y, Chen L, Liu Z, et al. Mitochondria-directed fluorescent probe for the detection of hydrogen peroxide near mitochondrial DNA. *Analytical Chemistry*. 2015;**87**:10579-10584. DOI: 10.1021/acs.analchem.5b03326
- [78] Hanson GT, Aggeler R, Oglesbee D, Cannon M, Capaldi RA, Tsien RY, et al. Investigating mitochondrial redox potential with redox-sensitive green

fluorescent protein indicators. The Journal of Biological Chemistry. 2004; **279**:13044-13053. DOI: 10.1074/jbc.M312846200

[79] Waypa GB, Marks JD, Guzy R, Mungai PT, Schriewer J, Dokic D, et al. Hypoxia triggers subcellular compartmental redox signaling in vascular smooth muscle cells. Circulation Research. 2010;**106**:526-535. DOI: 10.1161/CIRCRESAHA.109.206334

[80] Belousov VV, Fradkov AF, Lukyanov KA, Staroverov DB, Shakhbazov KS, Terskikh AV, et al. Genetically encoded fluorescent indicator for intracellular hydrogen peroxide. Nature Methods. 2006;**3**: 281-286. DOI: 10.1038/nmeth866

[81] Østergaard H, Henriksen A, Hansen FG, Winther JR. Shedding light on disulfide bond formation: Engineering a redox switch in green fluorescent protein. The EMBO Journal. 2001;**20**:5853-5862. DOI: 10.1093/emboj/20.21.5853

[82] Gutscher M, Pauleau A-L, Marty L, Brach T, Wabnitz GH, Samstag Y, et al. Real-time imaging of the intracellular glutathione redox potential. Nature Methods. 2008;**5**:553-559. DOI: 10.1038/nmeth.1212

[83] Albrecht SC, Barata AG, Großhans J, Teleman AA, Dick TP. In vivo mapping of hydrogen peroxide and oxidized glutathione reveals chemical and regional specificity of redox homeostasis. Cell Metabolism. 2011;**14**:819-829. DOI: 10.1016/j.cmet.2011.10.010

[84] Ermakova YG, Bilan DS, Matlashov ME, Mishina NM, Markvicheva KN, Subach OM, et al. Red fluorescent genetically encoded indicator for intracellular hydrogen peroxide. Nature Communications. 2014;**5**:1-9. DOI: 10.1038/ncomms6222

[85] Si F, Liu Y, Yan K, Zhong W. A mitochondrion targeting fluorescent

probe for imaging of intracellular superoxide radicals. Chemical Communications. 2015;**51**:7931-7934. DOI: 10.1039/C5CC01075F

[86] Yang K, Kolanowski JL, New EJ. Mitochondrially targeted fluorescent redox sensors. Interface Focus. 2017;**7**: 20160105. DOI: 10.1098/rsfs.2016.0105

[87] Arai S, Suzuki M, Park S-J, Yoo JS, Wang L, Kang N-Y, et al. Mitochondria-targeted fluorescent thermometer monitors intracellular temperature gradient. Chemical Communications (Cambridge, England). 2015;**51**: 8044-8047. DOI: 10.1039/c5cc01088h

[88] Chrétien D, Bénit P, Ha H-H, Keipert S, El-Khoury R, Chang Y-T, et al. Mitochondria are physiologically maintained at close to 50°C. PLOS Biology. 2018;**16**:e2003992. DOI: 10.1371/journal.pbio.2003992

[89] Jiang N, Fan J, Zhang S, Wu T, Wang J, Gao P, et al. Dual mode monitoring probe for mitochondrial viscosity in single cell. Sensors and Actuators B: Chemical. 2014;**190**:685-693. DOI: 10.1016/j.snb.2013.09.062

[90] Hell SW, Wichmann J. Breaking the diffraction resolution limit by stimulated emission: Stimulated-emission-depletion fluorescence microscopy. Optics Letters. 1994;**19**: 780-782. DOI: 10.1364/OL.19.000780

[91] Ishigaki M, Iketani M, Sugaya M, Takahashi M, Tanaka M, Hattori S, et al. STED super-resolution imaging of mitochondria labeled with TMRM in living cells. Mitochondrion. 2016;**28**: 79-87. DOI: 10.1016/j.mito.2016.03.009

[92] Wang C, Taki M, Sato Y, Tamura Y, Yaginuma H, Okada Y, et al. A photostable fluorescent marker for the superresolution live imaging of the dynamic structure of the mitochondrial cristae. PNAS. 2019;**116**:15817-15822. DOI: 10.1073/pnas.1905924116